13th ewtec 2019 Proceedings of the 13th European Wave and Tidal Energy Conference 1-6 Sept 2019, Naples, Italy

An efficient numerical framework for the assessment of free surface effects on crossflow tidal turbines

Milo Feinberg, Pál Schmitt, James Donegan and Jarlath McEntee

Abstract—**Cross-flow turbine technology is an interesting alternative to the more common horizontal axis turbine design for tidal or river flow environments. One important feature of marine hydrokinetic turbines operating in shallow water is the interaction with the free surface. Blockage can increase power output dramatically and must be accounted for accurately during the design process. However, the simulation of cross flow turbines is already computationally demanding due to the complex flow features and standard free surface simulation tools like the Volume of Fluid method would further increase the computational burden. Most simulations thus employ a slip surface condition, neglecting the complex interactions between the free surface deformation and blockage. This paper presents the application of a new numerical wave current tank to efficiently take free surface effects into account. First results show significant differences between cases employing the slip surface and the new numerical flume for power output and lift and drag coefficients.**

Index Terms—**cross-flow turbine, computational fluid dynamics (CFD), blockage, free surface effects**

I. Introduction

CROSS-FLOW turbine technology offers a number of advantages for marine hydrokinetic applications. In addition to the designs inherent durability, the low, rectangular profile of Ocean Renewable Power Company's (ORPC) advanced cross-flow turbine technology makes it well suited to many shallower river and tidal sites, and lends itself to cheaper operational costs and easier installation.

However, cross-flow turbine technology presents a number of technical challenges to the designer. Chief among these is the difficulty of developing reliable hydrodynamic models which can predict performance and direct design efforts and optimization campaigns.

Cross-flow turbines such as the RivGen® and TidGen® devices developed by ORPC differ in their mode of operation from conventional horizontal axis turbines [1]–[3]. The behavior of cross-flow turbines is inherently transient and periodic. As a result the quasi-steady-state simplifications often used to model horizontal axis turbines [4] are not applicable to the design of cross-flow turbines [5]. Long run-times are required to resolve the wake development and a sufficient number of rotations must be run for the turbine to reach a fully converged periodic behavior. Properly simulating the detaching and reattaching boundary layers required for accurate performance predictions is a considerable challenge and computationally costly. Some authors have successfully applied Large Eddy Simulations (LES) or Detached Eddy Simulation (DES) methods to cross flow turbines but for the commercial application to full scale prototypes the computational cost is still prohibitively high [6]–[8].

Commercial models like ORPC's RivGen® turbine are designed to be installed in rivers which are often shallow [3] and will consequently be affected during the operation by the free surface. The blockage caused by the turbine creates changes in surface elevation and thus affects the operating point of the turbine [9]. Correcting simulations or tank tests for blockage, even when limited to wall confined tests and ignoring the free surface, is complex and only recently have methods been developed which provide reasonable accuracy [10]. Optimization tools taking the free surface effects into account are required for accurately assessing the performance of cross-flow turbines in shallow domains. The standard application for the simulation of free surface effects is the Volume of Fluid (VoF) method because of its versatility and ability to resolve complex breaking waves and multiphase flows. The application of VoF methods requires a fine spatial and temporal resolution of the entire free surface region in the computational domain and solving computationally intensive species transport and interface compression methods, thus increasing the computational burden significantly compared to wall bounded single phase flows.

This study presents a numerical wave tank based on a special free surface boundary condition which avoids the need for a fine resolution of the free surface and additional transport equations while still able to simulate free surface effects. The paper is organized in the following sections. Section 2 presents the numerical wave tank, the underlying solver and wave and current generating capability. The third, fourth, and fifth sections present a test case, discussion of the simulation method, initial results, and a comparison between a closed tank for conventional optimisation simulations and the new simulations considering the free surface. The last section presents conclusions and an outlook to future work.

II. The solver

The numerical wave tank presented in this section is based on the potentialfreeSurfaceFoam solver from

Paper ID number: 1517- THM. This work was supported by the European Union under the TAIODE Project, H2020 grant No. 727465.

M. Feinberg, P. Schmitt, J. Donegan, J. McEntee are with ORPC Ireland Ltd. Bridge House, Baggot Street Upper Dublin 4, D04 X2P1, Ireland (e-mail: m.feinberg@orpc.co).

the OpenFOAM toolbox [11]. The solver tracks surface elevation using a variable ζ on the patch describing the water surface. Surface elevation is related to presssure using the simple hydrostatic relation $\zeta = p/(\rho g)$ with ρ the fluid density, p pressure and g acceleration due to gravity.

The current and wave making capability is added to potentialfreeSurfaceFoam following the concept as described [12], [13].

A RANS model includes the following impulse equation:

$$\frac{\partial(\rho \mathbf{U})}{\partial t} + \nabla \cdot (\rho \mathbf{U}\mathbf{U}) = -\nabla p + \nabla \cdot \mathbf{T} + \rho \mathbf{F}_b \qquad (1)$$

where t is time, $\mathbf{U}$ the fluid velocity, p the fluid pressure, ρ the fluid density, $\mathbf{F}_b$ the external forces such as gravity, and the viscous stress tensor $\mathbf{T} = \mu \nabla^2 \mathbf{U} + \frac{1}{3}\nabla(\nabla \cdot \mathbf{U})$, with the dynamic viscosity μ. To implement the impulse sources for wave and current generation, as well as a numerical beach for wave absorption, three terms are added to Eq. (1):

- $r_w \rho \mathbf{a}_{wm}$: This is the source term used for wave generation, where r_w is a binary scalar variable that defines the wavemaker region and $\mathbf{a}_{wm}$ is the acceleration input to the wavemaker at each cell centre within $r_w = 1$. This term is based on the implementation of an internal wavemaker in [12].
- $r_c \rho \frac{\mathbf{U_t} - \mathbf{U}}{\Delta t}$: This is the source term used for current generation, where r_c is a binary scalar variable that defines the current generation region. At each cell centre within $r_c = 1$, the acceleration input is defined through the difference between the velocity field $\mathbf{U}$ and a target velocity field $\mathbf{U_t}$.
- $s\vec{n}_z \rho \mathbf{U}$: This describes a dissipation term used to implement a numerical beach, where the variable s, with unit $[\mathrm{s}^{-1}]$, controls the strength of the dissipation [14]. Compared to the implementation in [12] and [14], in this study the beach only acts in the vertical, z-direction, to dissipate the waves, while allowing for a steady current flow in x-direction.

Augmenting Eq. (1) with these three terms yields the adapted impulse equation:

$$\frac{\partial(\rho \mathbf{U})}{\partial t} + \nabla \cdot (\rho \mathbf{U}\mathbf{U}) = -\nabla p + \nabla \cdot \mathbf{T} + \rho \mathbf{F}_b + r_w \rho \mathbf{a}_{wm} + r_c \rho \frac{\mathbf{U_t} - \mathbf{U}}{\Delta t} + s\vec{n}_z \rho \mathbf{U} \qquad (2)$$

III. Tank Layout and Simulations

Figure 1 presents the setup of the numerical wave tank. The ends of the domain are connected using a cyclic boundary condition to mimic a flume and prevent any mass loss. A current generator provides any additional momentum required to maintain a constant inflow velocity and is at the far left of the domain between the upstream and downstream beaches.

The tank's open channel is sized to loosely approximate ORPC's test site on the Kvichak River and extends 36 m upstream of the turbine and 108 m downstream of the turbine for a total length of 144 m. An upstream beach of 20 m and a downstream beach of 40 m are used in these simulations. The main purpose of the beaches is to absorb the relatively short waves caused by the foils passing near the surface and other instabilities caused by periodic changes in the turbine blockage. The overall domain size was chosen by a parameter study to ensure negligible influence of the domain length on the turbine's performance and to permit beaches large enough to prevent the reflection of waves at the inlet and outlet. It should be noted that since most of the cells are concentrated in the near vicinity of the turbine, domain length has a very limited influence on computational cost.

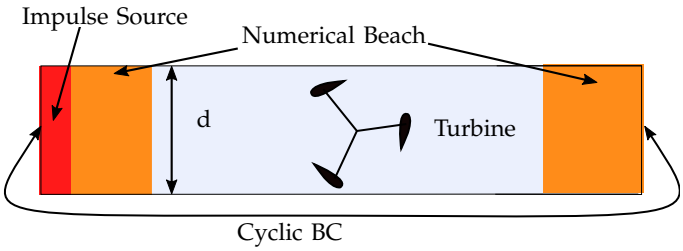

Fig. 1. Computational domain used for the present simulations. The turbine is placed in the middle of the test section. Upstream and downstream a beach dampens waves, but the current imposed by the current generator (colour) passes undisturbed.

The turbine used in these simulations is a 2D representation of ORPC's RivGen® 1.0 prototype turbine, a 50 kW device with two turbines of maximum radius $R = 0.75m$ and length $L = 4.1m$. The turbine has 4 foils with a chord length of $c = 0.2m$ and a NACA 63 series profile modified to have a thickened trailing edge for improved durability. Many features of the turbine geometry cannot be represented well in a 2D simulation, however, the shaft and the longitudinal members of the chassis are included. The RivGen® 1.0 was tested in the Kvichak River in Alaska during the summer of 2014.

Five simulations were completed with water depths from 5.0m to 12.5m representing the normal range of operating depths for the RivGen® Power System. A simulation was run at the water depth of 5.5m to match the conditions measured at the Akaska test site. An additional run at a depth of 22.5m was conducted representing the RivGen's operation in a separate deep-water deployment configuration. All simulations were run at a tip-speed ratio of $\lambda = 2.5$. This operating condition was chosen as representative of the turbine's usual operating condition, and is near the peak power point of the turbine.

To evaluate the effect of a free surface boundary condition on the results, the same 6 meshes were repeated as wall-bounded simulations, where the free surface boundary was replaced with a slip surface condition. In all cases, a no slip surface condition was applied to the bottom of the computational domain to simulate the effects of the riverbed on the turbine. While experimental data is not publicly available, ORPC does have data on the power output of its field deployment which demonstrate similar trends to those illustrated in this paper and can be used for continued validation of the methods presented here.

IV. Mesh and Simulation Parameters

A mesh and timestep convergence study was not carried out for this turbine geometry. For mesh settings, ORPC relied on the results of a convergence study performed on its RivGen® 2.0 Commercial Power System which has roughly similar diameter, chord length, and solidity to the RivGen® 1.0 prototype. The recommendations gleaned from this convergence study have proven to be robust for cross-flow turbines varying significantly in size, solidity, and Reynolds number. Similar studies performed on geometries ranging from model scale cross-flow turbines to ORPC's largest largest TidGen® turbine have led to similar conclusions about required mesh density and time-step size. ORPC believes the results presented here should be sufficiently accurate for the purpose of testing a novel free surface modeling technique.

The foils of cross-flow turbine's are exposed to a wide range of angles of attack and consequently experience periodic separation and reattachment of the flow. For meaningful prediction of stall behavior, critical to accurate performance prediction, the first cell height on the foils was selected to ensure a maximum $Y+$ value of approximately 1. Maintaining a thick layer of flow-aligned cells near the foils is required to properly resolve the behavior of boundary layers subjected to dynamic, adverse pressure gradients. A thick region of prismatic cells was built around the foil surfaces with 30 layers and a cell-to-cell expansion ratio of 1.15. As seen in Figure 2, the regions of the mesh within one chord length of the foil maintain a very high level of refinement to ensure resolution of the vortices shed by the foil during stall. All meshes were generated using snappyHexMesh, one of OpenFOAM's native meshing utilities.

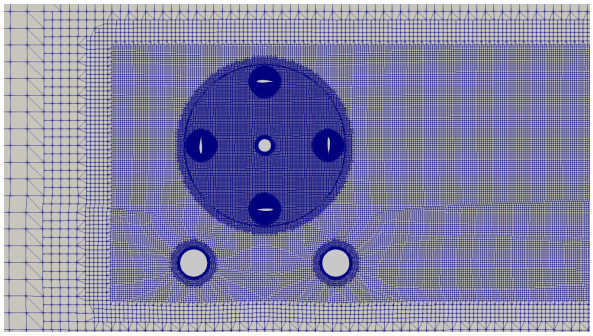

Fig. 2. Detail of the mesh in the region of the turbine.

A mesh refinement study was conducted on the upper boundary of the mesh and it was found that no additional refinement was required at the free surface. The base mesh, which is sized to resolve the far field wake, proved to be more than sufficient for the low amplitude waves generated by the turbine. The base mesh edge length is approximately $\frac{1}{25}$th of the smallest wave lengths observed.

The meshes have high quality criteria with a maximum non-orthogonality value of 49.5 and maximum skewness of 0.89. Second-order accurate, upwind schemes were used for the spatial discretization of the momentum equation and turbulence properties with cell limiters applied to the turbulence properties to ensure boundedness. The implicit, first-order accurate Euler scheme is used for the temporal discretization.

A time step equivalent to a $\frac{1}{2}$ degree of rotation was selected based on the RivGen® 2.0 convergence study. Time steps as coarse as 8 deg. of rotation can achieve average torque values within 5% of the converged value. However, they often show significant inaccuracy in their predictions of peak torque, the orbital angle at which peak torque occurs, and may fail to achieve the correct balance of power production between the upstream and downstream portions of a foil's path. Higher fidelity is required to resolve the finer physics of the stall and make meaningful comparisons between foil profiles, and other geometry changes.

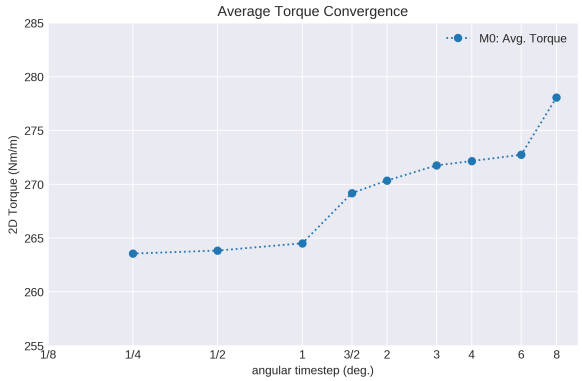

Fig. 3. A fine time step is required to accurately resolve the torque curves of a cross-flow turbine.

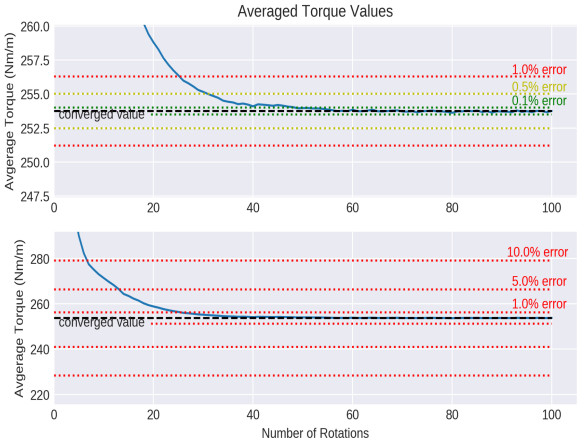

Fig. 4. Torque convergence of a cross-flow turbine at a tip-speed ratio of 2.50. The top and bottom plots show the same curve with different scaling in the y-axis for legibility.

A run time corresponding to 30 revolutions was chosen as appropriate for a turbine operating at a tip-speed ratio of 2.5. The number of revolutions required to reach a converged solution varies with tip-speed ratio due to the relationship between tip-speed ratio and turbine drag coefficient. To determine the required number of revolutions for convergence, a simulation was run through 100 revolutions. After 60 revolutions, the results stop changing (or rather all changes are negligible and stochastic, indicating the presence of minor numerical noise). From the simulation it was

found that 26 revolutions were required to achieve an error less than 1% in the average torque and 50 revolutions for an error less than 0.1%. 30 revolutions, with an error of approximately 0.5% in average torque was chosen as the practical limit for a simulation run time, and used for all the simulations presented here.

V. Results

Investigations of turbines with momentum theory demonstrate that restriction of the domain, whether through solid boundaries or a combination of solid boundaries and a free surface, increase the theoretical performance [15]. In a constrained domain, more water is forced through the turbine, resulting in greater power extraction and greater drag. In such conditions, turbine performance may exceed the canonical Betz limit [15]. This phenomenon can be seen in Figure 5, with the power predicted for the slip surface case demonstrating performance in excess of the Betz limit at a water depth of 5 m.

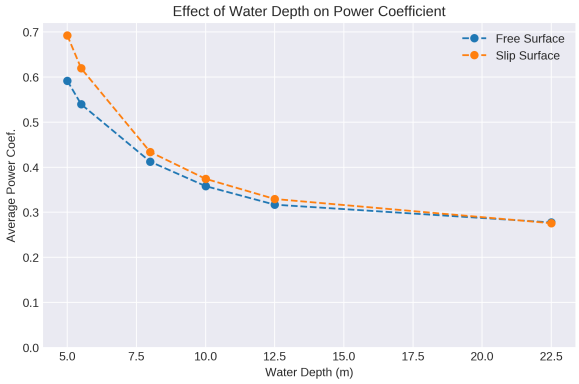

Fig. 5. Coefficient of power for varying depths for free surface and wall bounded simulations.

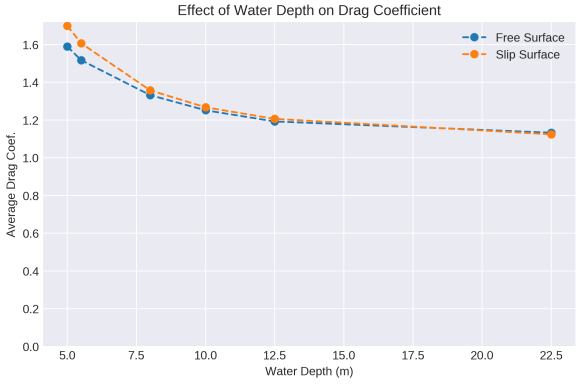

Fig. 6. Coefficient of drag for varying depths for free surface and wall bounded simulations.

At greater water depths, the difference between the free surface and slip surface condition is negligible. The differences in power extraction and drag, and the effect on the free surface profile are minimal. The power coefficient predicted for the turbine at a 22.5 m of water depth is 0.257 for the free surface case, and 0.256 for the wall bounded case. Similar agreement is found in the drag predictions where the wall bounded case and free surface cases show turbine drag coefficients of 1.125 and 1.133 respectively. The effect of the turbine on the free surface at such a high water depth is also minimal as can be seen in Figure 8, with a maximum wave height from peak to trough of 2 cm.

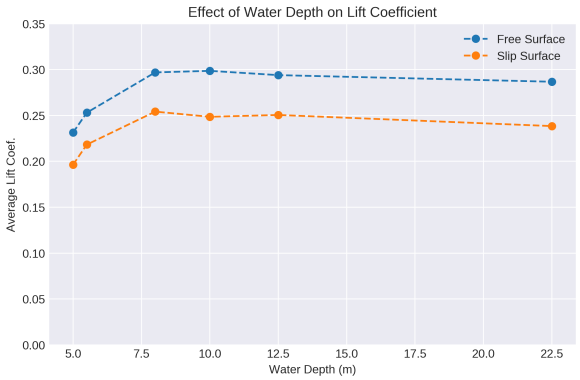

Fig. 7. Coefficient of lift for varying depths for free surface and wall bounded simulations.

In shallower sites, however, the turbine induces a significant standing wave over the turbine with increased water height upstream and decreased water height downstream of the turbine. This phenomenon, reproduced in the simulation, was evident during field tests conducted by ORPC in 2014 and 2015. The surface profile for a water depth of 5.5 m, as seen in Figure 8, shows a significant wave height, from peak to trough, of approximately 25 cm over the turbine. The development of this bore over the turbine results in a significant reduction in power production compared to the wall bounded cases. At a water depth of 5 m, the wall bounded and free surfaces cases have power coefficients of 0.692 and 0.592 respectively; a difference of nearly 15%. Similarly, the turbine drag coefficients for the wall bounded and free surfaces cases at 5 m water depth are 1.700 and 1.590 respectively. Correctly modeling the blockage imposed by the free surface is thus essential to accurate estimations of performance and structural loads. The disagreement between predictions made with these different boundary conditions is relatively small for deep water cases, but once the water depth is below 8 m the two methods diverge significantly in their predictions.

The effect of the water depth and boundary conditions on the lift coefficient is also considerable, see Figure 7. Oddly, however, the two curves do not converge at greater water depths and instead show a more or less constant offset. The origin of this peculiarity is currently under investigation.

Variation in water depth clearly has a significant effect on turbine performance and structural loads. For the free surface case the power generated in 5 m of water depth is greater than the power generated by the same turbine with the same inflow speed at 22.5 m of water depth by 213% and the drag loads increase by a 140%. The gains are even more extreme for the wall bounded case with an increase in performance by 251% and drag by 151%. While not directly comparable to these simplified 2D simulations, ORPC's field test data shows similar behavior in response to changes in

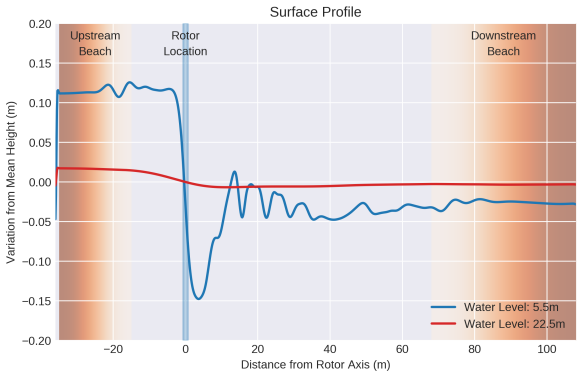

Fig. 8. Comparison of the surface elevation in the open channel of water depth 5.5m and water depth 22.5m after introduction of the turbine. The blue region shows the location in the plot that corresponds to the surface profile directly above the turbine. The upstream and downstream beaches are shown in orange.

operating water depth.

The effect of changes in water depth on performance is visible in the torque curves presented in Figure 9, which shows a single foil's coefficient of torque over a complete rotation as effected by water depth. The maximum coefficient of torque occurs for an angle of about 110 deg. with 0 deg. corresponding to the foil being at the 12 o'clock position and rotating in a counter clockwise direction. The highest water level of 22.5 m resulted in a maximum coefficient of torque produced by the foil of 0.175, a water level of only 12.5 m increased the coefficient to 0.18, further drops in water level over 10m to 8m and 5.5 m further increased the coefficient to 0.26. A change of water level between 5.5 and 5 m still increases the top levels to 0.28.

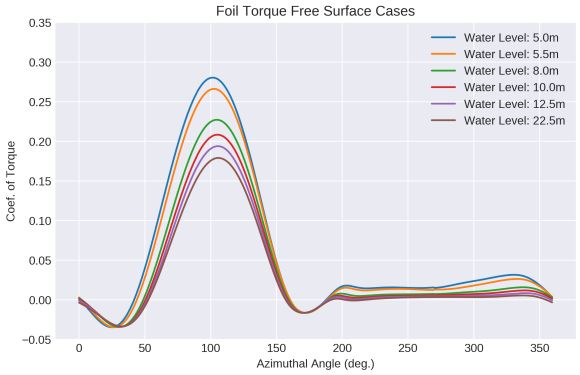

Fig. 9. Normalized foil torque for varying depths for free surace simulations.

A similar but more dramatic progression is seen for simulations performed using the wall bounded conditions as seen in Figure 10. A value of 0.18 is still similar to the free surface case, however for a tank height of 5.5 m the torque coefficient reaches values of 0.31 which is significantly more than the 0.27 obtained for the free surface case. For the 5 m water level the values are 0.32 compared to 0.28 for the free surface case.

For both the free surface and wall bounded simulations, the shape of the torque curves strongly resemble one another. For example, a reasonable facsimile of the

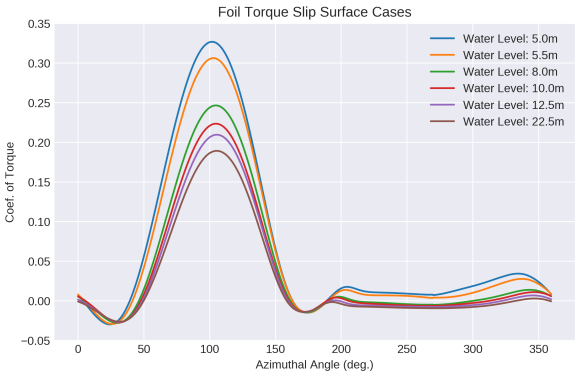

Fig. 10. Normalized foil torque for varying depths for wall bounded simulations.

torque curve at 5.5 m water depth could be constructed by simply applying a scaling factor to one of the other torque curves. This feature of the curves indicates to the authors that the primary change between these cases is not in the development of lift and drag forces on the foils, but rather a variation in the mean water velocity through the turbine. Hence the variation in boundary conditions both in type and proximity to the turbine are primarily changing the large scale momentum balance of the flow field.

Despite this relatively simple interaction between macro-performance metrics and the free surface simulation, at shallow water depths the free surface itself is quite dynamic and interacts considerably with the turbine and its wake. The surface profile shows periodic shedding of waves both upstream and downstream from the standing wave over the turbine. The magnitude of the effect can be gleaned from Figure 11 which shows the surface profile plotted on the same axis 18 times per rotation for the last 5 rotations.

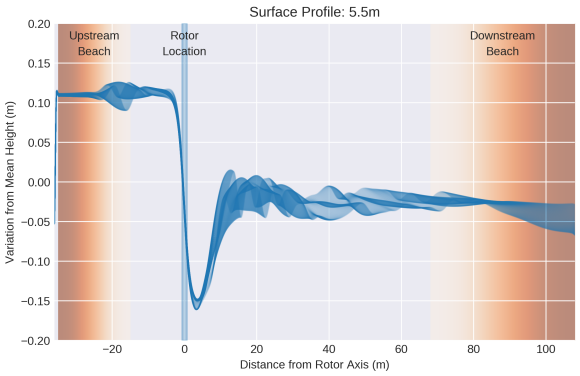

Fig. 11. Surface profile plotted every 20 deg. of rotation for the last 5 revolutions. Darker areas indicate areas where the surface profile is more persistence.

The wake of the turbine also shows periodic shedding which aligns with the free surface waves downstream of the turbine. The areas of low pressure and high velocity visible in Figure 12 near the surface correspond to local depressions in the free surface, and areas of low pressure and higher velocity correspond to local elevations.

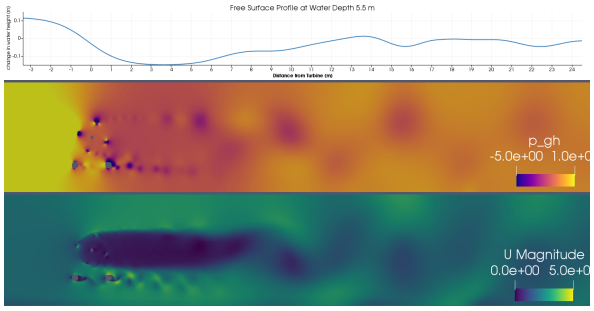

Fig. 12. Periodic shedding downstream of the turbine. **Top:** surface elevation from mean water depth (m). **Middle:** dynamic pressure field normalized by density (p/ρ). **Bottom:** Velocity field (m/s).

VI. Conclusions

This paper presented an efficient wave current interaction simulation toolbox and a first application to a cross-flow tidal turbine. The simulation methodology is shown to be capable of producing phenomena that are predicted in the literature and observed in testing such as increases in turbine power production, drag, the creation of a standing wave which varies with water depth. It is demonstrated that it is possible to take the free surface into account using a methodology that imposes negligible additional computational burden.

Some issues remain with the correct definition of the inflow velocity and careful experimental validation is required. 2D turbines, while providing a useful, low cost option for testing a new methodology, are not sufficient for full validation of the approach. In the future this setup with a more complete 3D turbine geometry will be validated against ORPC's field test data and used for wave current interaction studies to test the effect of swell waves for coastal installation of the RivGen® technology.

The simulations conducted show significant differences in the drag, lift, and power coefficients found for typical engineering applications. For turbines installed in shallow waters, these effects are significant and must be simulated accurately. Blockage corrections based on wall boundaries are insufficient. Accurately evaluating the loads of turbines in shallow waters is essential to improving the performance of ORPC's future turbine designs, as well as reducing risk through better prediction of the loads applied to the structure. The method will also be useful in evaluating potential installation sites and may allow ORPC to provide its customers with more accurate estimates of the expected power and the levelized cost of electricity (LCOE). Since these effects appear to related to blockage and momentum balance, these methods will find useful application in the design or evaluation of any marine hydro-kinetic device, or in fact any subsea system, operating in shallow waters.

References

[1] T. Harries, A. Kwan, J. Brammer, and R. Falconer, "Physical testing of performance characteristics of a novel drag-driven vertical axis tidal stream turbine; with comparisons to a conventional savonius," *International Journal of Marine Energy*, vol. 14, pp. 215 – 228, 2016. [Online]. Available: http://www.sciencedirect.com/science/article/pii/S2214166916300054

[2] P. Bachant and M. Wosnik, "Performance measurements of cylindrical- and spherical-helical cross-flow marine hydrokinetic turbines, with estimates of exergy efficiency," *Renewable Energy*, vol. 74, pp. 318–325, 2015, cited By 10. [Online]. Available: https://www.scopus.com/inward/record.uri?eid=2-s2.0-84906810263&doi=10.1016%2fj.renene.2014.07.049&partnerID=40&md5=83dca2dea39d5e432e4852f7974d7269

[3] D. Forbush, B. Polagye, J. Thomson, L. Kilcher, J. Donegan, and J. McEntee, "Performance characterization of a cross-flow hydrokinetic turbine in sheared inflow," *International Journal of Marine Energy*, vol. 16, pp. 150 – 161, 2016. [Online]. Available: http://www.sciencedirect.com/science/article/pii/S2214166916300455

[4] P. M. Singh and Y.-D. Choi, "Shape design and numerical analysis on a 1mw tidal current turbine for the south-western coast of korea," *Renewable Energy*, vol. 68, pp. 485 – 493, 2014. [Online]. Available: http://www.sciencedirect.com/science/article/pii/S0960148114001232

[5] M. Kear, B. Evans, R. Ellis, and S. Rolland, "Computational aerodynamic optimisation of vertical axis wind turbine blades," *Applied Mathematical Modelling*, vol. 40, no. 2, pp. 1038 – 1051, 2016. [Online]. Available: http://www.sciencedirect.com/science/article/pii/S0307904X15003984

[6] L. Priegue and T. Stoesser, "The influence of blade roughness on the performance of a vertical axis tidal turbine," *International Journal of Marine Energy*, vol. 17, pp. 136 – 146, 2017. [Online]. Available: http://www.sciencedirect.com/science/article/pii/S2214166917300073

[7] A. Posa, C. M. Parker, M. C. Leftwich, and E. Balaras, "Wake structure of a single vertical axis wind turbine," *International Journal of Heat and Fluid Flow*, vol. 61, Part A, pp. 75 – 84, 2016, sI TSFP9 special issue. [Online]. Available: http://www.sciencedirect.com/science/article/pii/S0142727X16300285

[8] H. Lei, D. Zhou, Y. Bao, Y. Li, and Z. Han, "Three-dimensional improved delayed detached eddy simulation of a two-bladed vertical axis wind turbine," *Energy Conversion and Management*, vol. 133, pp. 235 – 248, 2017. [Online]. Available: http://www.sciencedirect.com/science/article/pii/S0196890416310767

[9] C. Vogel, G. Houlsby, and R. Willden, "Effect of free surface deformation on the extractable power of a finite width turbine array," *Renewable Energy*, vol. 88, pp. 317 – 324, 2016. [Online]. Available: http://www.sciencedirect.com/science/article/pii/S0960148115304717

[10] T. Kinsey and G. Dumas, "Impact of channel blockage on the performance of axial and cross-flow hydrokinetic turbines," *Renewable Energy*, vol. 103, pp. 239 – 254, 2017. [Online]. Available: http://www.sciencedirect.com/science/article/pii/S0960148116309843

[11] G. M. Paredes, T. Tang, and J. Andric, *Application of dynamic meshes to potentialFreeSurfaceFoam to solve for 6DOF floating body motions*, 2012.

[12] P. Schmitt, C. Windt, J. Davidson, J. Ringwood, and T. Whittaker, "The efficient application of an impulse source wavemaker to cfd simulations," *Preprints 2019, 2019010222 (doi: 10.20944/preprints201901.0222.v1)*, 2019, under review.

[13] C. Windt, J. Davidson, P. Schmitt, and J. Ringwood, "Development of an impulse source-based wave-current interaction (wci) model," in *6th European Conference on Computational Mechanics (ECCM 6)7th European Conference on Computational Fluid Dynamics (ECFD 7)*, 6 2018.

[14] P. Schmitt and B. Elsaesser, "A Review of Wave Makers for 3D numerical Simulations," in *Preceedings of the 6th International Conference on Computational Methods in Marine Engineering*, 2015, pp. 437–446.

[15] G. T. Houlsby, S. Draper, and M. L. G. Oldfield, "Application of linear momentum actuator disc theory to open channel flow," University of Oxford, Department of Engineering Science, Parks Road, Oxford, OX1 3PJ, U.K., Tech. Rep., 2008.